SBAS Enhancement Using an Independent Monitor Station in a Local Area

Duojie Weng[1], **Wu Chen**[1]

[1] The Hong Kong Polytechnic University

Abstract

Different approaches have been developed to monitor the integrity of the Global Positioning System (GPS). The individual approaches rely on conservative error bounds and faces great challenges in meeting stringent integrity requirements set by the International Civil Aviation Organization (ICAO). These approaches, in fact, do not compete with one another but complement one another. We propose the vertical integration of the Satellite-Based Augmentation System (SBAS) and a local monitor station in this study. When the SBAS data deviate from the local monitor, users are informed to revert to the error bounds that are directly determined from SBAS data. Otherwise, the validation criterion that the error of the SBAS corrected solution is within a threshold is exploited to tighten the SBAS error bounds. The algorithm to integrate the SBAS with the independent monitor station is described, and its performance is evaluated based on simulations and real observations. The test results show that the vertical protection level (VPL) is reduced on average from 17.60 m to 11.27 m, i.e., a 30.3 % reduction in VPL while the integrity is guaranteed.

Keywords Integrity, Integration, Local monitor, SBAS

Introduction

Global Positioning System (GPS) enables a receiver to determine positions using satellite-to-user distances, which can be affected by several known errors. These errors can be reduced significantly with Differential GPS (DGPS) technologies or various models, meeting different accuracy requirements from several meters to 1-2 centimeters (Weng et al. 2015). GPS has thus been found in diverse applications such as transportation, agriculture and surveying. However, the integrity provided by GPS itself is not sufficient for safety critical applications. Although the control segment of GPS can detect and exclude some anomalies after 30 minutes after they happen, the

detection capacity, i.e., the latency, is insufficient for safety-critical users. For example, the control segment of GPS cannot satisfy the requirements for Approaches with Vertical Guidance I (APV-I) operation, which requires alerts should be delivered to users in 6 seconds (RTCA 2006).

Different integrity monitoring methods have been studied. The system-level integrity monitoring is provided by GPS stations throughout the world. Many GPS anomalies are difficult to be detected due to the limitation of sparsely distributed stations. Much denser stations are deployed in new satellite systems, and better integrity performance is anticipated for these new satellite systems (Oehler et al. 2004; Chen et al. 2017). For GPS, the integrity can be enhanced when GPS is augmented by the additional ground stations. In the past two decades, two distinct systems have been developed: Ground-Based Augmentation System (GBAS) for a local area and Satellite-Based Augmentation System (SBAS) for a wide area. These systems can mitigate most system errors, including satellite orbit, satellite clock and ionospheric errors, and the detection capacities can be improved. However, the user receiver errors, such as multipath cannot be mitigated using GBAS or SBAS. Even without the external information, the integrity can still be monitored in receivers by using a method that is often referred to as Receiver Autonomous Integrity Monitoring (RAIM). The concept of RAIM is to check the consistency among redundant measurements in the user receivers, and thus to detect and exclude faulty measurements (Ochieng et al. 2003). RAIM is indispensable since it monitors all error sources that affect the position solution. In particular, it monitors the user-receiver related errors such as multipath, interference and receiver failures, which are beyond the scope of other systems (Brown 1997; Wang and Ober 2009).

Integrity monitoring systems provide integrity information using various algorithms based on different data sources. These systems do not compete but complement one another. Various integrity monitoring systems can and should work together. In a previous study, RAIM was used in SBAS receivers to enhance the integrity of the SBAS position solution (Oliveira et al. 2009). In another study, the GBAS-like parameters are generated from a local monitor, enabling users to calculate the Protection Level (PL) for the SBAS positioning errors (Rife et al. 2005; Walter et al. 2005; Shively et al. 2006).

The potential benefits of integrating different integrity monitoring methods are: 1) One integrity system can detect anomalies in other integrity monitoring systems. For example, the GBAS can monitor localized ionospheric anomalies in a local area, which are possibly unobservable to the SBAS. 2) The error bounds can be reduced by using integrity data from different methods. In other words, the trust in GPS data can be improved when they are consistent with additional monitors. 3) The integrity requirements can be allocated to different integrity systems, and integrity requirements for each method can be relaxed. We present the vertical integration of SBAS and a local monitor station in this study. The first two benefits of integrating integrity monitoring methods are demonstrated later.

Compensating SBAS with a Local Monitor Station

The overview of SBAS is introduced first. The architecture of the integration and the model are then described in detail. The detection of anomalies and the tightening of error bounds are described later. The implementation issues are discussed in the last subsection.

Overview of SBAS

SBAS improves the navigation performance through the integration of external information. Figure 1 illustrates the concept of SBAS. The GPS measurements taken by reference stations are sent to the master station. Since the location of reference stations are known, the master station can generate corrections for the satellite clock error, the orbit error and the ionospheric delay, respectively. Essentially, the master station can generate the integrity information, e.g., error bounds for various errors. Both the corrections and the integrity data are relayed to users via the geostationary satellites. The data enable users to determine accurate positions and to evaluate the integrity.

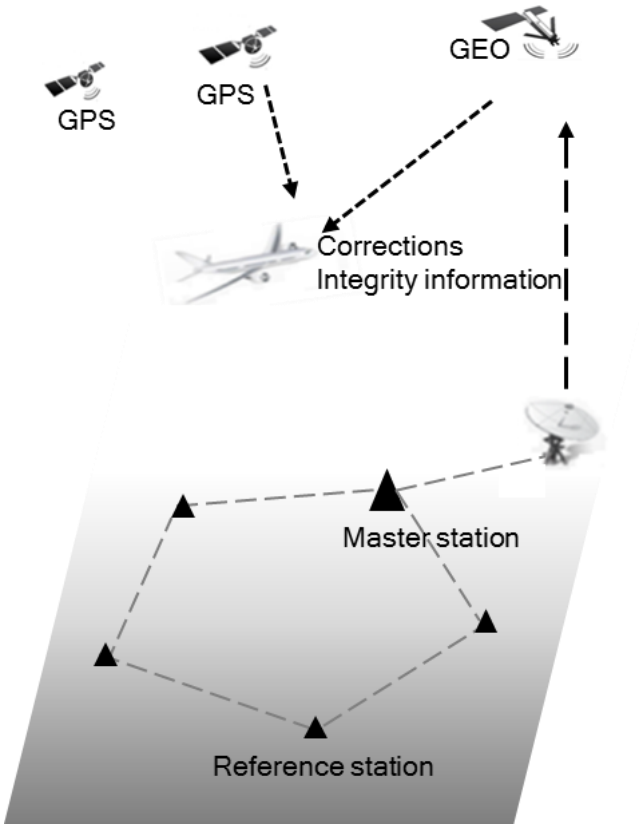

Fig. 1 Illustration of the SBAS components

Currently, SBAS has been developed in a number of countries. The operational SBAS includes the Wide Area Augmentation System (WAAS) in the United States, European Geostationary Navigation Overlay Service (EGNOS) in Europe, and Multi-functional Satellite Augmentation System (MSAS) in Japan (Manabe et al. 2008; Seynat et al. 2009). In the coming years, there will be a surge of new SBAS: Differential Corrections and Monitoring (SDCM) in Russia and GPS-Aided Geo-Augmented Navigation (GAGAN) in India. The SBAS is also being considered in China, South Korea, and Australia (Cao et al. 2012; Bang et al. 2016; Choy et al. 2017).

The user equipment applies the SBAS corrections to the GPS measurements. The residuals after applying SBAS data are

$$\varepsilon_i = \varepsilon_{flt,i} + \varepsilon_{UIRE,i} + \varepsilon_{tropo,i} + \varepsilon_{air,i} \quad (1)$$

where i is the index for the satellite, $i = 1,2 \cdots n$; ε_{flt}, ε_{UIRE} and ε_{tropo} account for the fast and long-term correction error, user ionospheric range error, and tropospheric error, respectively, and ε_{air} is the airborne receiver error. SBAS also broadcasts integrity information to users, and this enables receivers to calculate the error bounds σ_{flt}, σ_{UIRE} and σ_{tropo} accounting for ε_{flt}, ε_{UIRE} and ε_{tropo} respectively. The sum of the ranging error variances is

$$\sigma_i^2 = \sigma_{flt,i}^2 + \sigma_{UIRE,i}^2 + \sigma_{tropo,i}^2 + \sigma_{air,i}^2 \quad (2)$$

where σ_i^2 is the variance of the ranging error for satellite i, and σ_{air}^2 is the variance of the airborne receiver errors.

The SBAS receiver combines the ranging variances and the satellite geometry to calculate the position-domain error bound

$$VPL = K_{ffmd}\sqrt{\sum_{i=1}^{n} S_{vert,i}^2 \sigma_i^2} \quad (3)$$

where $S_{vert,i}$ is the vertical component of the projection matrix for satellite i and K_{ffmd} is a multiplier specified by the given integrity risk:

$$K_{ffmd} = Q^{-1}(1 - I_{req}/2) \quad (4)$$

where Q is the cumulative distribution function of the standard Gaussian distribution. Equations (3) and (4) show that the protection level is determined by different error bounds in the range domain, the satellite geometry, and a multiplier associated with the integrity risk. In particular, the availability degradation is mainly attributed to the inflated error bounds from SBAS: σ_{flt}, σ_{UIRE} and σ_{tropo}.

The existing SBAS tends to inflate error bounds to sufficiently address all known threats such as the receiver anomalies in reference stations, ionospheric irregularities and satellite signal deformations (Pullen et al. 2007; Blanch et al. 2014). SBAS can thus now meet requirements of APV-I approaches when the inflated sigma is applied (Comp et al. 1998; Walter et al. 2003). However, the availability degradation is still a difficult challenge when SBAS is used for more demanding operations, (Shively et al. 2006; Bang et al. 2016).

Vertical integration of SBAS with the local monitor station

The vertical integration of SBAS with a local monitor station is proposed in this study. The purpose of the vertical integration is to further enhance the integrity performance of SBAS in a local area, e.g., a local area of 37 km surrounding an airport. Figure 2 illustrates the concept of the integration. The SBAS data are first validated using measurements from the local single-frequency reference receivers. These receivers are installed within several kilometers of the airport. Then, the validation results are broadcast to nearby aircraft via a data link. If no anomalies are detected, the users will use the validation criterion to derive the new SBAS error distribution, which results in a tighter PL. If an anomaly is detected by the monitor station, proper actions will be taken, e.g., an alarm is transmitted to the aircraft. In this case, the aircraft will revert to the larger PL, which is directly determined from the SBAS.

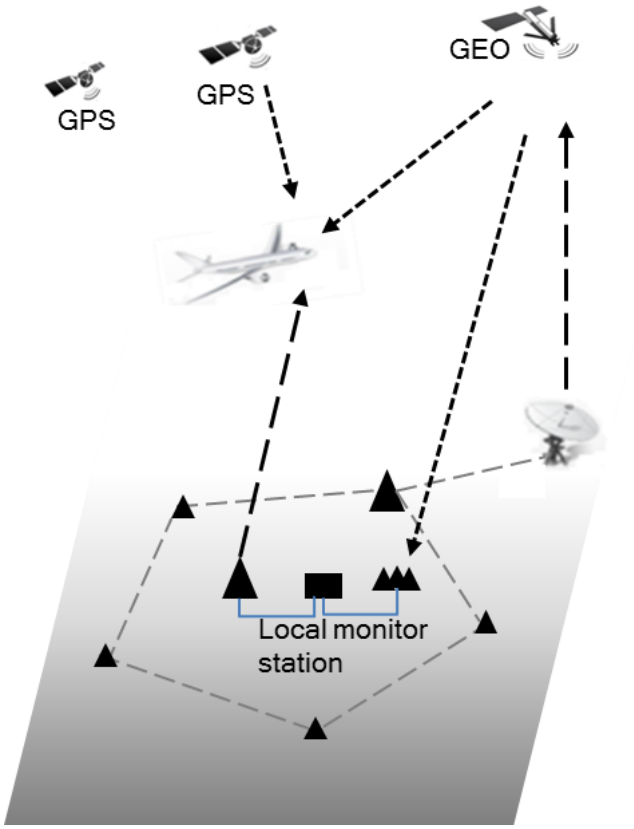

Fig. 2 Validation of SBAS data with the independent monitor station

Multiple reference receivers are installed within several kilometers of the airport. The reference receivers should be properly installed in the open area. These receivers need to be close enough to enable the calculation of the averaged pseudorange corrections for each satellite. However, the distances between the reference receivers should not be too close either, because the multipath effects are not independent otherwise.

Since the coordinates of reference receivers are precisely known, the pseudorange corrections can be generated by subtracting the computed range from the observed pseudorange. For each satellite, the pseudorange corrections are averaged across reference receivers. Receiver anomalies can be detected by comparing the averaged pseudorange correction with the pseudorange correction from each receiver (Dautermann et al. 2012; Wang et al. 2014).

For a fault-free receiver, the new pseudorange is calculated as the sum of the computed range and the averaged pseudorange correction. We assume that the local noise and multipath for different reference receivers are statistically independent. The effects of noise and multipath can thus be reduced when the new pseudorange is used. When the SBAS corrections are applied to the new pseudorange, an equation similar to (1) is obtained

$$\varepsilon_i = \varepsilon_{flt,i} + \varepsilon_{UIRE,i} + \varepsilon_{tropo,i} + \varepsilon_{r,i} \tag{5}$$

where ε_r is the averaged noise and multipath effects of reference receivers. If the reference receivers are connected to high-end antennas in the open area, the term ε_r mainly describes the measurement noise, and the noise level can be kept very small. If we define the SBAS system error as $\varepsilon_{s,i} = \varepsilon_{flt,i} + \varepsilon_{UIRE,i} + \varepsilon_{tropo,i}$, equation (5) can be represented by:

$$\varepsilon_i = \varepsilon_{s,i} + \varepsilon_{r,i} \tag{6}$$

where $\varepsilon_{s,i}$ is system error after applying SBAS corrections.

In (6), error $\varepsilon_{s,i}$ is the system error after applying SBAS corrections for satellite i, i.e., the residual in orbit error, clock error and ionospheric error, while $\varepsilon_{r,i}$ is for the local multipath and measurement noise experienced by local reference receivers. In other words, $\varepsilon_{s,i}$ (the SBAS system error) and $\varepsilon_{r,i}$ (local multipath and noise) represent different errors, and do not contain

common errors. We assume that $\varepsilon_{s,i}$ is statistically independent from $\varepsilon_{r,i}$. If there is no alarm raised, we will use this property to derive the new PDF of $\varepsilon_{s,i}$.

The monitor station solves for positions in a similar way as the airborne receiver does. The positioning error is a projection of measurement error $\boldsymbol{\varepsilon}$ into the position domain:

$$\boldsymbol{PE} = (\boldsymbol{G}^T\boldsymbol{W}\boldsymbol{G})^{-1}\boldsymbol{G}^T\boldsymbol{W}\cdot\boldsymbol{\varepsilon} = (\boldsymbol{G}^T\boldsymbol{W}\boldsymbol{G})^{-1}\boldsymbol{G}^T\boldsymbol{W}(\boldsymbol{\varepsilon}_s + \boldsymbol{\varepsilon}_r)$$

$$= \boldsymbol{PE}_s + \boldsymbol{PE}_r \tag{7}$$

where $\boldsymbol{G}$ is a coefficient matrix, containing partial derivatives representing directions of satellites, $\boldsymbol{W}$ is the diagonal weight matrix, and the main diagonal are defined as $w_{ii} = 1/\sigma_i^2$, $\boldsymbol{PE}_s$ is the positioning error caused by the SBAS system error, and $\boldsymbol{PE}_r$ is the positioning error caused by the local noise and multipath of reference receivers. Since the integrity requirement in the vertical direction is more stringent than that in the horizontal component for aviation navigation, we will focus on the vertical component in this study:

$$VPE = VPE_s + VPE_r \tag{8}$$

VPE_s and VPE_r are the projections of two independent measurement errors ε_s and ε_r into the position domain, respectively.

The SBAS system error VPE_s in (8) follows a normal distribution given by

$$p_s(VPE_s) = \frac{1}{\sqrt{2\pi}\sigma_{s,v}} e^{-\frac{1}{2}\left(\frac{VPE_s}{\sigma_{s,v}}\right)^2} \tag{9}$$

where $p_s(VPE_s)$ is the Probability Density Function (PDF) of VPE_s, and $\sigma_{s,v}$ is the inflated sigma for the SBAS system error. VPE_r is vertical positioning error caused by the local noise and multipath of reference receivers, which it is bounded by the distribution

$$p_r(VPE_r) = \frac{1}{\sqrt{2\pi}\sigma_{r,v}} e^{-\frac{1}{2}(\frac{VPE_r}{\sigma_{r,v}})^2} \tag{10}$$

where $p_r(VPE_r)$ is the PDF of VPE_r, and $\sigma_{r,v}$ is the error bound for vertical position errors caused by local noise and multipath of reference receivers.

As discussed, VPE_s and VPE_r are two independent variables. Since two random variables are independent if and only if the joint PDF is equal to the product of the PDFs of each variable, the joint PDF of VPE_s and VPE_r can be written as

$$p(VPE_s, VPE_r) = p_s(VPE_s)p_r(VPE_r) = \frac{1}{2\pi\sigma_{s,v}\sigma_{r,v}} e^{-\frac{1}{2}\left(\frac{VPE_s^2}{\sigma_{s,v}^2}+\frac{VPE_r^2}{\sigma_{r,v}^2}\right)} \quad (11)$$

where $p(VPE_s, VPE_r)$ is the joint PDF of VPE_s and VPE_r.

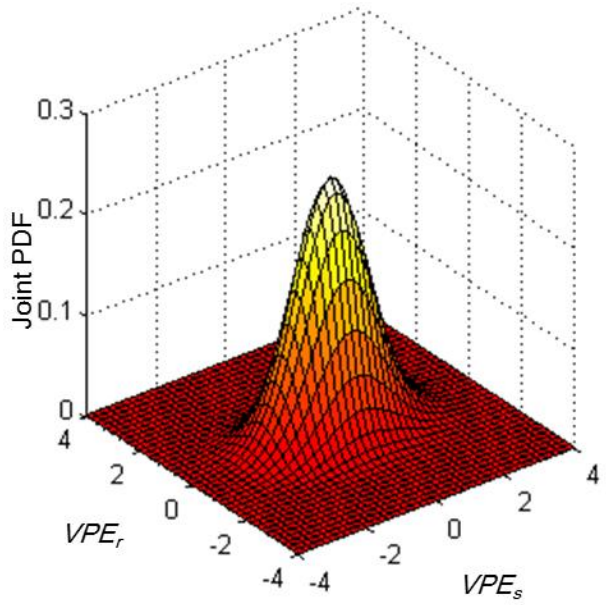

Fig. 3 Illustration of the joint PDF of two independent variables

Figure 3 illustrates the joint PDF, which is defined in the entire $VPE_s - VPE_r$ plane. The total volume under the surface $p(VPE_s, VPE_r)$ and above the plane is 1. The probability that the point (VPE_s, VPE_r) lies in a specified region of the plane can be calculated as the double integration of the joint PDF over the corresponding region. We will later describe how the faults

are detected in the $VPE_s - VPE_r$ plane and how to tighten the SBAS error bound using the local monitor.

Detecting SBAS anomalies and tightening the error bound

To determine if there are anomalies in the SBAS data, the test statistic VPE is compared with a threshold T_v

$$T_v = K_{fa}\sigma_{total,v} = K_{fa}\sqrt{\sigma_{r,v}^2 + \sigma_{s,v}^2} \tag{12}$$

where K_{fa} is the multiplier determined by the probability of false alarm P_{fa}; $\sigma_{total,v}$ is the sigma of the total measurement error, which is calculated by $\sigma_{total,v} = \sqrt{\sigma_{r,v}^2 + \sigma_{s,v}^2}$.

Figure 4 illustrates how to detect SBAS anomalies. When the test statistic VPE exceeds the threshold T_v, the point (VPE_s, VPE_r) lies in the brown region in the figure. For this point, the monitor station issues a warning message to inform the users; in response, the users will revert to using the PL that is directly determined from the SBAS data.

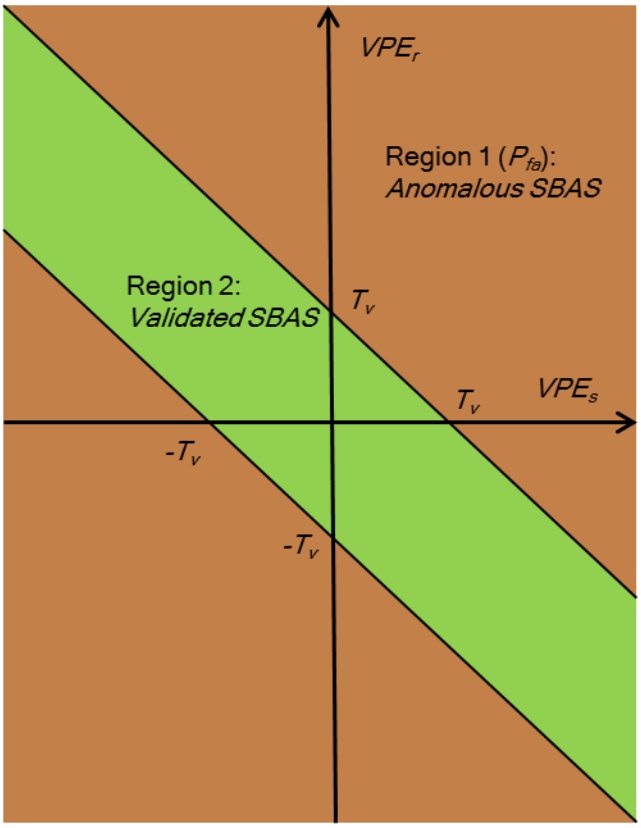

Fig. 4 Detection of anomalies in SBAS corrections

When the SBAS is validated by the local monitor, VPE_s is constrained by the inequality of $|VPE_s + VPE_r| < T_v$. For this case, the point (VPE_s, VPE_r) lies in the green region in Figure 4. Under this condition, the conditional PDF of VPE_s is given by

$$p_{s,n}(VPE_s) = \frac{\int_{-VPE_s-T_v}^{-VPE_s+T_v} p(VPE_s,VPE_r)dVPE_r}{1-P_{fa}} \tag{13}$$

where $p_{s,n}(VPE_s)$ is the new PDF for the SBAS error VPE_s. As shown, the new PDF for the error VPE_s is calculated by normalizing the marginal PDF of VPE_s. The denominator in (13) is the probability that the point lies in the green region $(1 - P_{fa})$, whereas the numerator is the marginal PDF of VPE_s.

As discussed in (11), the VPE_s is independent from VPE_r, and the joint probability density function is their product $p(VPE_s, VPE_r) = p_s(VPE_s)p_r(VPE_r)$. Therefore, we have:

$$p_{s,n}(VPE_s) = \frac{\int_{-VPE_s-T_v}^{-VPE_s+T_v} p_r\,(VPE_r)p_s(VPE_s)dVPE_r}{1-P_{fa}}$$

$$= p_s(VPE_s)\frac{\int_{-VPE_s-T_v}^{-VPE_s+T_v} p_r\,(VPE_r)dVPE_r}{1-P_{fa}}$$

$$= p_s(VPE_s)\cdot SF(VPE_s) \tag{14}$$

where $SF(VPE_s)$ is defined as a scale factor function of VPE_s, namely $SF(VPE_s) = \frac{\int_{-VPE_s-T_v}^{-VPE_s+T_v} p_r(VPE_r)dVPE_r}{1-P_{fa}}$. The new PDF of VPE_s is the product of the original PDF $p_s(VPE_s)$ and a scale factor function.

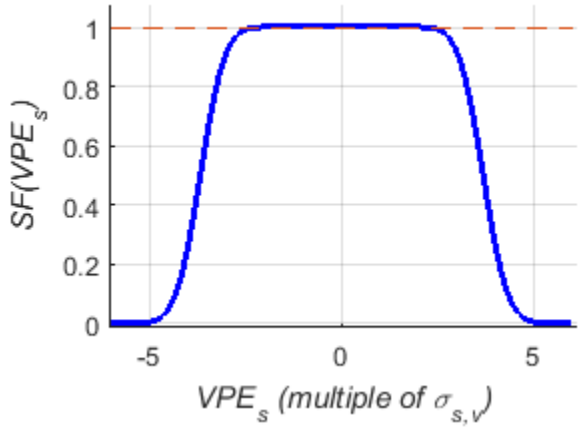

Fig. 5 Scale factor as a function of VPE_s ($\sigma_{r,v} = 0.5 \cdot \sigma_{s,v}$, $P_{fa} = 10^{-4}$)

Figure 5 illustrates the scale factor function based on the following assumptions: $\sigma_{r,v} = 0.5 \cdot \sigma_{s,v}$; $P_{fa} = 10^{-3}$. When VPE_s is near the zero point, the factor is close to 1.0, and the new PDF is similar to the original one. When VPE_s is bounded away from the zero point, as shown in the figure, the factor rapidly decreases, particularly when VPE_s approaches threshold T_v.

With the new PDF determined from (14), the new VPL (VPL_n) can be determined with the given integrity risk

$$\int_{-VPL_n}^{VPL_n} p_{s,n}(VPE_s) = 1 - IR \tag{15}$$

where IR is the integrity risk requirement. Because the new PDF has tighter tails, the new VPL will be reduced.

Implementation issues

As discussed, the monitor station detects anomalies and improves the SBAS error bounds. Both are performed in the position domain. The prerequisite is that the satellites used in the user's position solution are identical to those used in the monitor station. A feasible solution is to enumerate all possible subsets of satellites at the monitor station. If the user does not use up to two of satellites viewed by the reference receivers, the monitor station should consider

$$m = \sum_{k=n-2}^{n} \binom{n}{k} \tag{16}$$

subsets of satellites (Lee et al. 2011).

In the integration concept, the radio frequency (RF) data link from the monitor station to the aircraft is required. The type of data link should be carefully developed since it is a critical factor that affects the integrity requirement in terms of the time to alert. One possible solution is to develop a specific data link for this purpose. These data link should be certified for use in aircraft navigation, as performed in the GBAS. One possible alternative is to transmit the data via the VHF data broadcast of the GBAS, but the data to be transmitted must be modified to fit the GBAS format (Rife et al. 2005; Shively et al. 2006).

We should also consider the types of messages delivered from the monitor station to the aircraft. Equation (14) shows that the new PDF is not a Gaussian distribution represented by a simple standard deviation. To reduce the amount of data, we broadcast the parameters in (14) instead of the resulting distribution of correction errors. In other words, for each subset, a flag is

broadcast to the users to inform them whether an anomaly is detected. The monitor station also broadcasts two parameters $\sigma_{r,v}$ and P_{fa} to users. In response, the SBAS users calculate $\sigma_{s,v}$ for the SBAS correction errors and calculate the detection threshold (T_v). With these parameters, the SBAS user reconstructs the new distribution of SBAS correction errors.

Simulation

The integration of SBAS with the local monitor station reduces the PL, and the improvement is sensitive to the quality of local measurements. Thus, a simulation is performed to evaluate the effects of different receiver qualities on the PL. In the simulation, the probability of false alarm P_{fa} is assumed to be 10^{-3}, which results in $T_V = 3.29\sigma_{total,v}$. The aircraft receivers can continue using the PL that is directly determined from the SBAS when the alarm was received.

The term $\sigma_{r,v}$ accounts for local receiver errors, whereas the SBAS error bound $\sigma_{s,v}$ accounts for many potential threats such as an ionospheric error and satellite orbit error. Five situations are considered in the simulation, i.e., $\sigma_{r,v} = 0.2 \cdot K \cdot \sigma_{s,v}, (K = 1,2 \dots 5)$. This simulation enables us to analyze how the tails are reduced by using measurements with different qualities. For each situation, the new PDFs are calculated from (14), and the PL is obtained from (15).

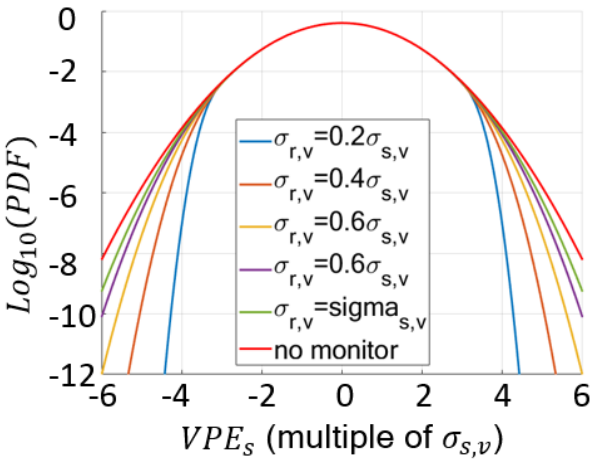

Fig. 6 New PDFs *vs.* original PDF

The possible large errors of VPE_s have been screened out by the monitor station. When there is no alarm raised from the monitor station, the new PDF can be obtained from (14). Figure 6 shows the original PDF (red curve) with a Gaussian tail and five new PDFs from different monitor stations. As shown in the figure, the tails in new PDFs are reduced significantly when we used the monitor stations. In other words, the probability of large errors of VPE_s has been reduced. We can also see that more improvement is achieved when better local measurements are used, which suggests that high-quality measurements are required to guarantee the integration performance. When the pseudoranges from multiple receivers are combined, as suggested in the previous section, the noise level of local measurements can be improved, and better performance can be achieved.

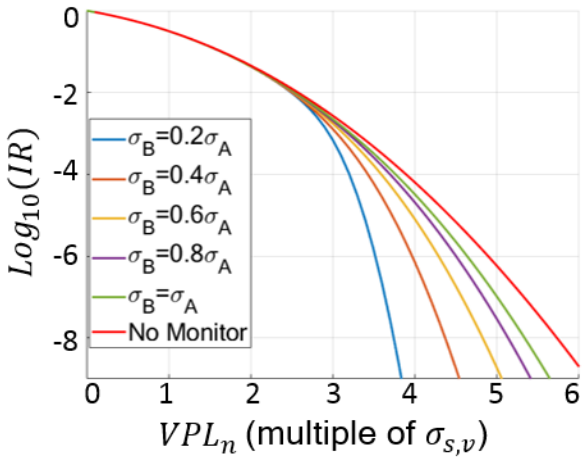

Fig. 7 Integrity risk *vs.* protection level for different monitors

With a given integrity risk, the new PL can be derived when the new PDFs in Figure 6 are applied in (15). Figure 7 shows the relationship between the PL and the integrity risk for different monitor stations. The PL decreases when the SBAS is integrated with the monitor station, and the improvement in PL is more significant when better-quality measurements are used to validate the SBAS data. As shown, for the APV-I operation with the integrity risk of 10^{-7}, the original VPL is $5.33 \cdot \sigma_{s,v}$. The VPL is reduced to $3.87 \cdot \sigma_{s,v}$, $4.37 \cdot \sigma_{s,v}$, $4.72 \cdot \sigma_{s,v}$, $4.94 \cdot \sigma_{s,v}$ and $5.09 \cdot \sigma_{s,v}$ when five different monitor stations are used.

Experimental Results

The integration algorithm was assessed for 24 hours using observations from two Continuously Operating Reference Stations (CORS) on February 9, 2018 in America. The station CORB was selected as the monitor station, and the station LOY8 was selected as the user. The sampling interval of two stations is 1 second. Both stations are within the WAAS coverage. The baseline length between the two stations is 10.88 km. We only considered all satellites viewed by both stations, and the effects of different satellite subsets on the performance are beyond the scope of the assessment.

The WAAS data were verified using observations from the station CORB. The first step is to smooth the pseudorange measurements of CORB using a single-frequency filter with the smoothing time of 100 seconds (RTCA, 2017). Then, the WAAS message data were downloaded from the website and applied to reduce different pseudorange errors. The variance of residual errors in WAAS corrections is designated following the specification defined in RTCA (2006). The CORB station has a modern receiver with a simpler choke-ring antenna, and this reference receiver performance is classified as the Ground Accuracy Designator (GAD) B (RTCA, 2017). In this evaluation, the single reference receiver was used as the monitor station. If multiple reference receivers are used, the receiver noise could be significantly reduced, and better performance could be achieved.

Figure 8 shows the test statistic VPE of the station CORB and the corresponding threshold T_v determined with the false alarm probability of 10^{-3}. As shown, the test statistic was always within the threshold, and no alarm was declared during the period. In other words, the integration algorithm can be performed in nearby aircraft in the 24-hour period.

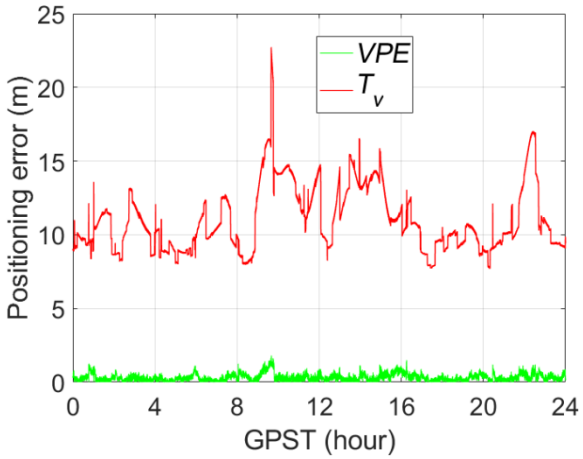

Fig. 8 Test statistic *vs.* threshold

Figure 9 shows the error bounds $\sigma_{r,v}$ and $\sigma_{s,v}$, which are evaluated at the monitor station CORB. The contribution of $\sigma_{r,v}$ is much smaller than that of $\sigma_{s,v}$. On average, $\sigma_{s,v}$ was 3.30 m, and $\sigma_{r,v}$ was 0.54 m. These parameters are provided to the LOY8 station (simulated user), which enables it to calculate the new protection level.

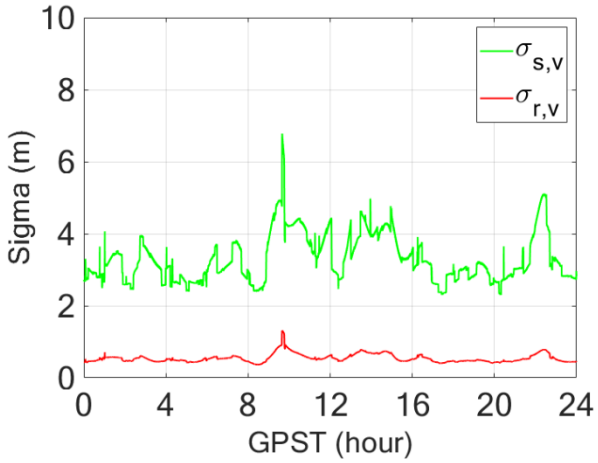

Fig. 9 Comparison of the error bounds

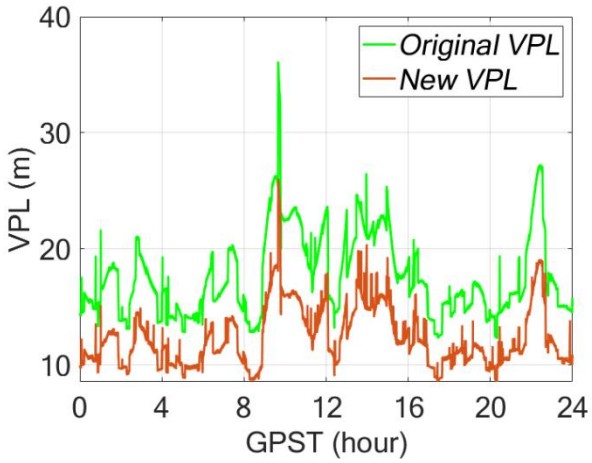

Fig. 10 Comparison of the original VPL with the new VPL

Two programs were developed to evaluate the performance of the proposed method. The first program does not use the monitor station (SBAS only), whereas the second program combines the SBAS with the monitor station (SBAS + monitor). Two types of VPL were calculated based on the assumption that the user (LOY8) was conducting the APV-I operation with the integrity requirement of 10-7. The original VPL was determined from (3), and the new VPL was determined from (15). Figure 10 compares the new VPL with the original VPL. The green curve represents the original VPLs using only SBAS, and the red curve represents the new VPLs using the local monitor station. For all of these observations, the positioning errors for the user LOY8 are bounded by the new PL. The average VPL is 17.60 m without using the monitor station. In contrast, the average VPL decreases to 12.27 m, i.e., 30.3 % reduction in VPL when the monitor station is used.

Conclusions

The integration of integrity monitoring systems is proposed in this study. The SBAS data is verified using the local monitor station to improve the integrity performance. The simulations demonstrate that the local monitor station decreases the PL. The performance of the local monitor

was also evaluated with real observations in North America, where the WAAS service was available. When the user positioning errors are bounded, the test results show that VPL is reduced from 17.60 m to 12.27 m. The described method can be extended to integrate other integrity monitoring systems. In fact, several integrity monitoring methods are available for users, and their integration will benefit civil aviation, particularly in terms of improved integrity performance.

In this study, the local monitor is utilized to reduce the PL of SBAS for the nominal case. Since multiple reference receivers are installed in the local monitor, the anomalies undetected by SBAS itself can be possibly addressed by the local monitor. The anomalies of SBAS are characterized by non-zero-mean biases or inflated sigma values, and therefore the model will be expanded in future work. The probability of abnormal events not detected or bounded by SBAS is extremely low, and sufficient SBAS data need to be processed.

The proposed method does require a data link from the local monitor station and the aircraft, which should satisfy the 6-second time requirement for APV and LPV operations. In future work, the data link should be carefully developed for use in aircraft navigation. Another challenge that requires special attention is how to integrate other integrity monitoring systems together. For example, the integration of RAIM with the distinct SBAS/GBAS should be investigated in the next step. Future work will also include dynamic aircraft tests, which are critical in validating the proposed algorithm.

Acknowledgements The work described in this paper was substantially supported by the National Key Research and Development Program of China (Project No. 2016YFB0502100, 2016YFB0502101) and the European Commission / Research Grants Council (RGC) Collaboration Scheme, which is sponsored by the Research Grants Council of Hong Kong Special Administrative Region, China (Project No. E-PolyU 501/16). The NOAA's National Geodetic Survey (NGS) is acknowledged for providing the data in this study. Two reviewers are thanked for their insightful comments.

References

Bang E, Lee J, Walter T and Lee J (2016) Preliminary availability assessment to support single-frequency SBAS development in the Korean region. GPS Solutions 20(3):299-312

Blanch J, Walter T, Enge P, Stern A, Altshuler E (2014) Evaluation of a Covariance-based Clock and Ephemeris Error Bounding Algorithm for SBAS. In: Proc. ION GNSS 2014, Institute of Navigation, Tampa, Florida, USA, September 8-12, 3270–3276

Brown, RG (1997) Solution of the two-failure GPS RAIM problem under worst case bias conditions: Parity space approach. Journal of Institute of Navigation 44(4):425-431

Cao Y, Zhou S, Hu X, Wu B, Zhou S, Liu L, Su R, Chang Z, He F, Zhou J (2012) The wide-area difference system for the regional satellite navigation system of COMPASS. Sci China Phys Mech Astron 55(7):1307–1315

Chen J, Huang Z, Li R (2017) Computation of satellite clock–ephemeris corrections using a priori knowledge for satellite-based augmentation system. GPS Solutions 21(2):663-673

Dautermann T, Felux M, Grosch A (2012) Approach service type D evaluation of the DLR GBAS testbed. GPS Solut 16(3):375-387

Choy S, Kuckartz J, Dempster AG, Rizos C, Higgins M (2017) GNSS satellite-based augmentation systems for Australia. GPS Solutions 21(3):835-848

Comp C et al. (1998) Demonstration of WAAS aircraft approach and landing in Alaska. In: Proc. ION GPS 1998, Institute of Navigation, Nashville, TN, USA, September 15-18, 177–184

Lee, J, Seo, J, Park YS, Pullen S, Enge P (2011) Ionospheric threat mitigation by geometry screening in Ground-Based Augmentation Systems. Journal of Aircraft 48(4):1422-1433

Manabe H (2008) Status of MSAS: MTSAT satellite-based augmentation system. In: Proc. ION GNSS 2008, Institute of Navigation, Savannah, GA, September 16-19, 1032–1059

Ochieng WY, Sauer K, Walsh D, Brodin G, Griffin S, Denney M (2003) GPS integrity and potential impact on aviation safety. The Journal of Navigation 56(1):51–65

Oehler V, Luongo F, Boyero J, Stalford R, Trautenberg HL, Hahn J, Amarillo F, Crisci M, Schlarmann B, Flamand JF (2004) The Galileo Integrity Concept. Pro. ION GNSS 2004, Institute of Navigation, Long Beach, CA, September, 604-615

Oliveira J and Tiberius C (2009) Quality Control in SBAS: Protection Levels and Reliability Levels. The Journal of Navigation 62(3):509-522

Pullen S and Enge P (2007) An overview of GBAS integrity monitoring with a focus on ionospheric spatial anomalies. Indian Journal of Radio & Space Physics 36(4):249-260

Rife J, Pullen S, Walter T, Enge P (2005) Vertical Protection Levels for A Local Airport Monitor for WAAS. Proc. ION 61st AM, Institute of Navigation, Cambridge, MA, USA, June 24-27, 745-758

RTCA (2006) Minimum operational performance standards for global positioning system/wide area augmentation system airborne equipment, RTCA DO-229D. RTCA, Inc., December 2006

RTCA (2017) Minimum operational performance standards for global positioning system for GPS Local Area Airborne Equipment, RTCA DO-253A. RTCA, Inc., July 2017

Seynat C, Flament D, Brocard D (2009) EGNOS Status Update. In: Proc. ION GNSS 2009, Institute of Navigation, Savannah, GA, USA, September 16-19, 3457-3483

Shively C, Niles R, Hsiao T (2006) Performance and availability analysis of a simple Local Airport Position Domain Monitor for WAAS. Navigation 53(2):97-108

Walter T, Enge P and DeCleene B (2003) Integrity Lessons from the WAAS Integrity Performance Panel (WIPP). In: Proc. ION NTM 2003, Institute of Navigation, Anaheim, CA, USA, January 22-24, 183-194

Walter T, Pullen S, Rife J (2005) The Advantages of Local Monitoring and VHF Data Broadcast for SBAS. In: Proc. of the European Navigation Conference GNSS 2005, Munich, Germany

Wang J, and Ober P (2009) On the availability of fault detection and exclusion in GNSS receiver autonomous integrity monitoring. Journal of Navigation 62(2): 251-261

Wang Z, Macabiau C, Zhang J, Escher AC (2014) Prediction and analysis of GBAS integrity monitoring availability at LinZhi airport. GPS Solut 18(1):27–40

Weng D, Ji S, Chen W (2015) Assessing and mitigating the effects of the ionospheric variability on DGPS. GPS Solutions 19(1):107–116

Author Biographies

Duojie Weng received the B.S. and M.S. degrees in electrical engineering from Hohai University, Nanjing, China in 2007 and 2010 and the Ph.D. degree from the Hong Kong Polytechnic University in 2016. He is currently a post-doctoral researcher at the Hong Kong Polytechnic University. His research interests include GNSS integrity monitoring, kinematic GPS, and sensor integration for various navigation systems.

Wu Chen is a Professor with the Hong Kong Polytechnic University. His interests include GNSS Applications on Transportation, Kinematic GPS, System Integration, GNSS Performance Evaluation, GPS Software Receiver, Regional GPS Network, Vehicle and Personal Navigation Systems, and Wireless Sensor Network.